Progress In Electromagnetics Research, Vol. 135, 373–390, 2013

PLRC AND ADE IMPLEMENTATIONS OF DRUDE-CRITICAL POINT DISPERSIVE MODEL FOR THE FDTD METHOD

Kyungwon Chun, Huioon Kim, Hyounggyu Kim, and Youngjoo Chung*

School of Information and Mechatronics, Gwangju Institute of Science and Technology (GIST), 123 Cheomdan-gwagiro, Buk-gu, Gwangju 500-712, Republic of Korea

Abstract—We describe the implementations of Drude-critical point model for describing dispersive media into finite difference time domain algorithm using piecewise-linear recursive-convolution and auxiliary differential equation methods. The advantages, accuracy and stability of both implementations are analyzed in detail. Both implementations were applied in studying the transmittance and reflectance of thin metal films, and excellent agreement is observed between analytical and numerical results.

1. INTRODUCTION

The field of plasmonics which explores the interaction of light with metals has gained tremendous interest over the past few years [1, 2]. Several numerical techniques have been proposed to study the interaction/propagation of electromagnetic waves with metals [3], and one of the most popular and widely accepted techniques is the finite-difference time-domain (FDTD) method [4]. FDTD being a time domain technique, offers several advantages particularly for the study of light-metal interaction since the frequency response of the system under study over a wide range of frequencies can be obtained with a single run of simulation.

The frequency-dependent electric permittivity is an important parameter to be known in advance when studying the frequency response of the material over a wide frequency range. Traditionally, Drude-Lorentz (DL) model which can well represent the optical

Received 22 November 2012, Accepted 7 December 2012, Scheduled 25 December 2012
* Corresponding author: Youngjoo Chung (ychung@gist.ac.kr).

properties of the metal originating from the interband and intraband transitions was the popular one and has been used to quantify the dispersion properties of the metal [5, 6]. In DL model, a large number of Lorentz oscillators can be used to model the line shape of the electric permittivity of the material over the frequency range of interest [7]. However, the accuracy improvement obtained via adding more Lorentz terms comes with a price. A large number of Lorentz terms lead to increased requirement of computational resources such as CPU power and memory [8].

Recently, Drude-critical point (DCP) model that consists of one Drude term and two critical point terms was proposed which can satisfactorily represent the electric permittivity of metals over a wide frequency range [7, 9]. From the computational perspective, DCP model is advantageous over DL model since the former requires only less number of terms. Since then, DCP model has been used to represent the electric permittivity of metals such as gold and others with good accuracy [10].

Several implementation techniques are available to model dispersive media in the FDTD algorithm. For example, Kelley and Luebbers [11] proposed a piecewise-linear recursive-convolution (PLRC) method to implement the Debye and Lorentz dispersive media and the results were compared to that of Luebbers et al. [12] which used the recursive-convolution (RC) method. Vial [13] implemented the DCP model by using RC method while Sullivan [14], Weedon and Rappaport [15] used the Z-transform technique to implement dispersive media into the FDTD algorithm. An auxiliary differential equation (ADE) technique to implement the Lorentz dispersive model was proposed [16] and it was shown by Okoniewski et al. [17] that the usage of the ADE scheme resulted in reduced computational burden compared to that of PLRC technique.

In this work, we will show the FDTD implementation of DCP dispersive model by using two popular techniques, i.e., PLRC and ADE. Memory requirements as well as the accuracy for each implementation are analyzed in detail. Numerical results are compared to that of analytical results for the case of reflection and transmission of light through thin metal films in order to validate the proposed implementation schemes.

2. FDTD IMPLEMENTATION

The DCP dispersive model expresses interband transitions featuring asymmetric line shapes with critical point terms instead of Lorentzian terms [7]. The relative electric permittivity as per the DCP model can

be written as

$$\epsilon_r(\omega) = \epsilon_\infty + \chi_D(\omega) + \sum_{p=1}^{2} \chi_p(\omega) \tag{1}$$

where ϵ_∞ is the relative electric permittivity at infinite frequency, $\chi_D(\omega)$ the Drude susceptibility, and $\chi_p(\omega)$ the critical point susceptibility. The Drude susceptibility is expressed as

$$\chi_D(\omega) = -\frac{\omega_D^2}{\omega^2 + i\gamma\omega} \tag{2}$$

where ω_D is the Drude pole frequency and γ the inverse of the pole relaxation time. Also, the critical point susceptibility is expressed as

$$\chi_p(\omega) = A_p \Omega_p \left(\frac{e^{i\phi_p}}{\Omega_p - \omega - i\Gamma_p} + \frac{e^{-i\phi_p}}{\Omega_p + \omega + i\Gamma_p} \right) \tag{3}$$

where A_p is the amplitude, ϕ_p the phase, $\hbar\Omega_p$ the energy gap, and Γ_p the broadening of the pole. The time dependence is described following the $e^{-i\omega t}$ convention. In the following, PLRC and ADE implementation of the DCP model is shown.

2.1. Numerical Implementation in PLRC

The PLRC method uses a linear approximation to evaluate the electric field $\mathbf{E}(t)$ over each time-stepping interval [11] and has better accuracy compared to the RC method which assumes a constant electric field over the time-stepping interval.

The equation for updating the electric field $\mathbf{E}^n$ at time-step $t = n\Delta t$ is

$$\begin{aligned}\mathbf{E}^{n+1} = {} & \frac{2\Delta t}{2\epsilon_0\left(\epsilon_\infty - \xi^0 + \chi^0\right) + \sigma\Delta t} \nabla \times \mathbf{H}^{n+1/2} + \frac{2\epsilon_0\left(\epsilon_\infty - \xi^0\right) - \sigma\Delta t}{2\epsilon_0(\epsilon_\infty - \xi^0 + \chi^0) + \sigma\Delta t} \mathbf{E}^n \\ & + \frac{2\epsilon_0}{2\epsilon_0\left(\epsilon_\infty - \xi^0 + \chi^0\right) + \sigma\Delta t} \mathbf{\Psi}^n \end{aligned} \tag{4}$$

where

$$\begin{aligned} \chi^0 &= \chi_D^0 + \Re\left(\sum_p \hat{\chi}_p^0\right) \\ \xi^0 &= \xi_D^0 + \Re\left(\sum_p \hat{\xi}_p^0\right) \\ \mathbf{\Psi}^n &= \mathbf{\Psi}_D^n + \Re\left(\sum_p \hat{\mathbf{\Psi}}_p^n\right). \end{aligned} \tag{5}$$

The exact forms of the variables on the right hand side of Eq. (5) are described in Sections 2.1.1 and 2.1.2. $\mathbf{\Psi}^n$ is the recursive accumulator which is the convolutional sum of electric field and temporal susceptibility. σ is the electrical conductivity, ϵ_0 is the vacuum permittivity, and Δt is the time-stepping interval. The "$\hat{}$" denotes a complex number. If we set ξ_D^0, $\hat{\xi}_p^0$, $\Delta\xi_D^0$, and $\Delta\hat{\xi}_p^0$ to 0, then Eqs. (4), (5), (9), (13) become identical to that of RC implementation in Vial [13].

2.1.1. The Drude Term

The time-domain susceptibility function $\chi_D(t)$ is obtained by inverse Fourier transformation of Eq. (2), yielding

$$\chi_D(t) = \frac{\omega_D^2}{\gamma}\left(1 - e^{-\gamma t}\right) U(t) \tag{6}$$

where $U(t)$ is the unit step function. Substituting Eq. (6) into the definition of χ^m and ξ^m shown in Kelley and Luebbers [11], we obtain the following equations

$$\begin{aligned} \chi_D^0 &= \frac{\omega_D^2}{\gamma^2}\left(e^{-\gamma\Delta t} + \gamma\Delta t - 1\right) \\ \xi_D^0 &= \chi_D^0\left(\frac{1}{1 - e^{\gamma\Delta t}} + \frac{1}{\gamma\Delta t}\right) - \frac{\omega_D^2}{\gamma^2}\left(1 - \frac{\gamma\Delta t}{2}\coth\frac{\gamma\Delta t}{2}\right) \end{aligned} \tag{7}$$

which are used for updating the electric field. The coefficients that are necessary for the recursive accumulator of the Drude pole are given by

$$\begin{aligned} \Delta\chi_D^0 &= -\frac{\omega_D^2}{\gamma^2}\left(1 - e^{-\gamma\Delta t}\right)^2 \\ \Delta\xi_D^0 &= \Delta\chi_D^0\left(\frac{1}{1 - e^{\gamma\Delta t}} + \frac{1}{\gamma\Delta t}\right). \end{aligned} \tag{8}$$

Also, the recursive accumulator $\mathbf{\Psi}_D^n$ for the Drude pole obeys the following recursion relation

$$\mathbf{\Psi}_D^{n+1} = \left(\Delta\chi_D^0 - \Delta\xi_D^0\right)\mathbf{E}^{n+1} + \Delta\xi_D^0\mathbf{E}^n + e^{-\gamma\Delta t}\mathbf{\Psi}_D^n. \tag{9}$$

2.1.2. Critical Point Terms

The time-domain susceptibility function $\chi_p(t)$ is obtained by inverse Fourier transformation of Eq. (3), and is written as

$$\chi_p(t) = 2A_p\Omega_p e^{-\Gamma_p t}\sin(\Omega_p t - \phi_p)U(t). \tag{10}$$

$\chi_p(t)$ has the form similar to the real-valued time-domain susceptibility function for the case of Lorentzian media and does not lead to a simple recursion relation for χ^m and ξ^m [11]. Hence we need to define a new complex-valued quasi-time-domain function [13]

$$\hat{\chi}_p(t) = 2iA_p\Omega_p e^{-\Gamma_p t - i(\Omega_p t - \phi_p)}U(t). \tag{11}$$

The form of $\hat{\chi}_p(t)$ is close to that for the Lorentzian case [11], thus the procedure detailed in the case of a combination of Drude and Lorentzian terms can be applied, and steps required for the numerical implementation of the critical point model can be derived similar to Vial and Laroche [18]. Substituting $\hat{\chi}_p(t)$ for $\chi(t)$ in the definition of χ^m and ξ^m, we obtain

$$\begin{aligned} \hat{\chi}_p^0 &= \frac{2iA_p\Omega_p e^{i\phi_p}\left(1 - e^{-\Delta t(\Gamma_p + i\Omega_p)}\right)}{\Gamma_p + i\Omega_p} \\ \hat{\xi}_p^0 &= \hat{\chi}_p^0\left(\frac{1}{1 - e^{\Delta t(\Gamma_p + i\Omega_p)}} + \frac{1}{\Delta t(\Gamma_p + i\Omega_p)}\right) \end{aligned} \tag{12}$$

for updating the electric field. The recursive accumulator for the critical point term becomes complex as in the case of Lorentz media. The recursion relation for the recursive accumulator of the pth critical point is written as

$$\hat{\mathbf{\Psi}}_p^{n+1} = \left(\Delta\hat{\chi}_p^0 - \Delta\hat{\xi}_p^0\right)\mathbf{E}^{n+1} + \Delta\hat{\xi}_p^0\mathbf{E}^n + e^{-\Delta t(\Gamma_p + i\Omega_p)}\hat{\mathbf{\Psi}}_p^n \tag{13}$$

with the following parameters

$$\begin{aligned} \Delta\hat{\chi}_p^0 &= \frac{2iA_p\Omega_p e^{i\phi_p}\left(1 - e^{-\Delta t(\Gamma_p + i\Omega_p)}\right)^2}{\Gamma_p + i\Omega_p} \\ \Delta\hat{\xi}_p^0 &= \Delta\hat{\chi}_p^0\left(\frac{1}{1 - e^{\Delta t(\Gamma_p + i\Omega_p)}} + \frac{1}{\Delta t(\Gamma_p + i\Omega_p)}\right). \end{aligned} \tag{14}$$

Thus, the PLRC scheme for modeling a DCP dispersive medium in the FDTD algorithm is essentially a four-step explicit procedure, and can be briefed as follows: Starting with the known values of $\mathbf{E}^n$, $\mathbf{\Psi}_D^n$, $\hat{\mathbf{\Psi}}_p^n$, $\mathbf{H}^{n+1/2}$, we first calculate $\mathbf{\Psi}^n$ using the last equation of Eq. (5) and then calculate $\mathbf{E}^{n+1}$ which is the updated electric field using Eq. (4). With the updated electric field, we can then update recursive accumulators for each pole using Eqs. (9) and (13). Finally, $\mathbf{H}^{n+3/2}$ is obtained from $\mathbf{H}^{n+1/2}$ and $\mathbf{E}^{n+1}$ in the usual manner from the Yee realization of Faraday's law, and this cycle repeats for every time-step.

2.2. Numerical Implementation in ADE

The ADE scheme is simpler than the PLRC scheme. Using the complex phasor notation, the differential form of Ampere's law can be expressed for a DCP medium as

$$\nabla \times \breve{\mathbf{H}} = -i\epsilon_0\epsilon_\infty\omega\breve{\mathbf{E}} - i\omega\breve{\mathbf{P}}_D - i\omega\sum_p \breve{\mathbf{P}}_p + \sigma\breve{\mathbf{E}} \tag{15}$$

where $\breve{\mathbf{P}}_D$ and $\breve{\mathbf{P}}_p$ are the polarization fields represented in the form of

$$\breve{\mathbf{P}}_D = \epsilon_0\chi_D(\omega)\breve{\mathbf{E}} \tag{16}$$

and

$$\breve{\mathbf{P}}_p = \epsilon_0\chi_p(\omega)\breve{\mathbf{E}}. \tag{17}$$

Here, "$\breve{}$" denotes the quantity in frequency domain. The inverse Fourier transformation of Eq. (15) can be implemented in FDTD at a fixed time $(n+1/2)\Delta t$ using the central differencing and semi-implicit scheme, where yet-to-be-computed fields at time-step $n+1$ are used to create an update formula for a field known at time-step n given by

$$\begin{aligned}\mathbf{E}^{n+1} \;=\; & \frac{2\Delta t}{2\epsilon_0\epsilon_\infty + \sigma\Delta t}\nabla\times\mathbf{H}^{n+1/2} - \frac{2\left(\mathbf{P}_D^{n+1} - \mathbf{P}_D^{n}\right)}{2\epsilon_0\epsilon_\infty + \sigma\Delta t} \\ & - \frac{2\sum_p\left(\mathbf{P}_p^{n+1} - \mathbf{P}_p^{n}\right)}{2\epsilon_0\epsilon_\infty + \sigma\Delta t} + \frac{2\epsilon_0\epsilon_\infty - \sigma\Delta t}{2\epsilon_0\epsilon_\infty + \sigma\Delta t}\mathbf{E}^n.\end{aligned} \tag{18}$$

This equation cannot be used to update electric field yet, since the right hand side of it contains yet-to-be-computed values of $\mathbf{P}_D^{n+1}$, $\mathbf{P}_p^{n+1}$. Thus we require auxiliary equations to compute those variables.

2.2.1. The Drude Term

The Drude term can be converted into a form suitable to be used in the time-stepping scheme by using the method introduced by Okoniewski and Okoniewska [19] without losing the second-order nature of the model. By applying the central differencing and semi-implicit scheme at n on the inverse Fourier transformation of Eq. (16), we get the equation for the Drude field at the time-step $n+1$ as

$$\mathbf{P}_D^{n+1} = a_0\mathbf{P}_D^{n-1} + a_1\mathbf{P}_D^{n} + a_2\left(\mathbf{E}^{n-1} + 2\mathbf{E}^{n} + \mathbf{E}^{n+1}\right) \tag{19}$$

where

$$\begin{aligned} a_0 &= \frac{\gamma\Delta t - 2}{\gamma\Delta t + 2} \\ a_1 &= \frac{4}{\gamma\Delta t + 2} \\ a_2 &= \frac{\Delta t^2\epsilon_0\omega_D^2}{2(\gamma\Delta t + 2)}. \end{aligned} \tag{20}$$

2.2.2. Critical Point Terms

By applying the central difference scheme at n on the inverse Fourier transformation of Eq. (17), we obtain the equation for critical point terms at time-step $n+1$ as

$$\mathbf{P}_p^{n+1} = b_{p,0}\mathbf{P}_p^{n-1} + b_{p,1}\mathbf{P}_p^{n} + b_{p,2}\mathbf{E}^{n-1} + b_{p,3}\mathbf{E}^{n} + b_{p,4}\mathbf{E}^{n+1} \tag{21}$$

where

$$\begin{aligned}
b_{p,0} &= -\frac{\Omega_p^2\Delta t^2 + (2-\Gamma_p\Delta t)^2}{\Omega_p^2\Delta t^2 + (2+\Gamma_p\Delta t)^2} \\
b_{p,1} &= 2\frac{4 - \left(\Gamma_p^2 + \Omega_p^2\right)\Delta t^2}{\Omega_p^2\Delta t^2 + (2+\Gamma_p\Delta t)^2} \\
b_{p,2} &= 2\epsilon_0 A_p\Omega_p\Delta t\frac{\Omega_p\Delta t\cos\phi_p + (2-\Gamma_p\Delta t)\sin\phi_p}{\Omega_p^2\Delta t^2 + (2+\Gamma_p\Delta t)^2} \\
b_{p,3} &= 4\epsilon_0 A_p\Omega_p\Delta t\frac{\Omega_p\Delta t\cos\phi_p - \Gamma_p\Delta t\sin\phi_p}{\Omega_p^2\Delta t^2 + (2+\Gamma_p\Delta t)^2} \\
b_{p,4} &= 2\epsilon_0 A_p\Omega_p\Delta t\frac{\Omega_p\Delta t\cos\phi_p - (2+\Gamma_p\Delta t)\sin\phi_p}{\Omega_p^2\Delta t^2 + (2+\Gamma_p\Delta t)^2}.
\end{aligned} \tag{22}$$

Substituting Eqs. (19), (21) into Eq. (18) and with few algebraic manipulation, we obtain the following explicit time-stepping relation for $\mathbf{E}$:

$$\begin{aligned}
\mathbf{E}^{n+1} = {} & c_0\nabla\times\mathbf{H}^{n+1/2} + c_1\left(-a_0\mathbf{P}_D^{n-1} + (1-a_1)\mathbf{P}_D^{n}\right) \\
& + c_1\sum_p\left(-b_{p,0}\mathbf{P}_p^{n-1} + (1-b_{p,1})\mathbf{P}_p^{n}\right) + c_2\mathbf{E}^{n-1} + c_3\mathbf{E}^{n}
\end{aligned} \tag{23}$$

where

$$\begin{aligned}
c_0 &= \frac{\Delta t}{\sigma\Delta t/2 + a_2 + \sum_p b_{p,4} + \epsilon_0\epsilon_\infty} \\
c_1 &= \frac{1}{\sigma\Delta t/2 + a_2 + \sum_p b_{p,4} + \epsilon_0\epsilon_\infty} \\
c_2 &= -\frac{a_2 + \sum_p b_{p,2}}{\sigma\Delta t/2 + a_2 + \sum_p b_{p,4} + \epsilon_0\epsilon_\infty} \\
c_3 &= -\frac{\sigma\Delta t/2 + 2a_2 + \sum_p b_{p,3} - \epsilon_0\epsilon_\infty}{\sigma\Delta t/2 + a_2 + \sum_p b_{p,4} + \epsilon_0\epsilon_\infty}.
\end{aligned} \tag{24}$$

The ADE scheme for modeling a DCP dispersive medium in the FDTD algorithm is a three-step fully explicit procedure. Starting with the known values of $\mathbf{E}^{n-1}$, $\mathbf{E}^{n}$, $\mathbf{P}_D^{n-1}$, $\mathbf{P}_D^{n}$, $\mathbf{P}_p^{n-1}$, $\mathbf{P}_p^{n}$, and $\mathbf{H}^{n+1/2}$,

we first calculate $\mathbf{E}^{n+1}$ using Eq. (23). Second, we calculate $\mathbf{P}_D^{n+1}$ and $\mathbf{P}_p^{n+1}$ using Eqs. (19) and (21), respectively, along with the value of $\mathbf{E}^{n+1}$ that was just computed. Finally, $\mathbf{H}^{n+3/2}$ is obtained from $\mathbf{H}^{n+1/2}$ and $\mathbf{E}^{n+1}$ in the usual manner from the Yee realization of Faraday's law, and this cycle repeats for every FDTD time-step. Note that in contrast with the PLRC scheme, the ADE implementation uses only real parameters, and hence it can be used for updating complex electromagnetic field as well by just changing the type of field variables.

3. MEMORY USAGE

Figures 1 and 2, respectively, show the schematic flowcharts which describes the components used for PLRC and ADE implementations between two successive time-marching steps. In calculating Drude as well as critical point terms, the PLRC implementation requires a smaller number of components and about 22% less memory than ADE.

The ADE method, however, has an advantage of requiring relatively fewer arithmetic operations to the PLRC method as shown in figures where the number of arrows, which represent arithmetic

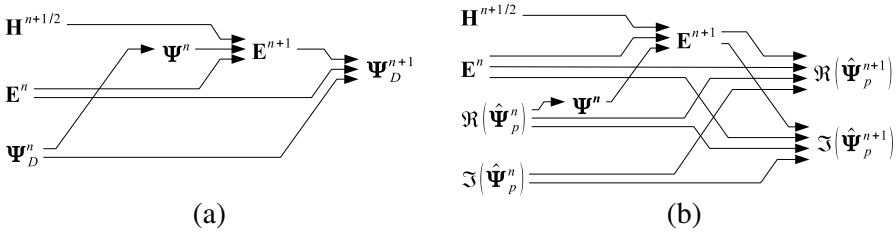

Figure 1. Schematic flowcharts for (a) a Drude term and (b) a critical point term for the PLRC implementation of DCP model.

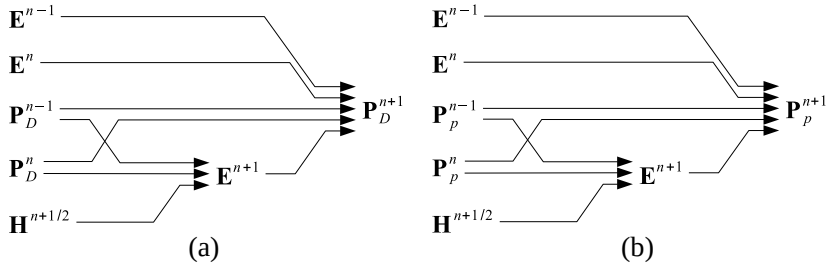

Figure 2. Schematic flowcharts for (a) a Drude term and (b) a critical point term for the ADE implementation of DCP model.

operations in Fig. 2 is fewer than shown in Fig. 1. It can also be implemented more efficiently than the PLRC method since the schematic flows for Drude and critical point terms in the ADE scheme are identical to each other and have fewer number of steps compared to the PLRC scheme as shown in Fig. 2. This is another advantage of the ADE method over the PLRC method.

4. ACCURACY ESTIMATES

We can determine the accuracy of each implementation scheme using the generalized time-sampled relation ship between polarization and electric fields [20, 21] given by

$$g_0\mathbf{P}^{n-1} + g_1\mathbf{P}^n + g_2\mathbf{P}^{n+1} = \epsilon_0\left(h_0\mathbf{E}^{n-1} + h_1\mathbf{E}^n + h_2\mathbf{E}^{n+1}\right). \quad (25)$$

Substituting the time harmonic solutions $\mathbf{P}^n = \mathbf{P}_0 e^{-i\omega n\Delta t}$, $\mathbf{E}^n = \mathbf{E}_0 e^{-i\omega n\Delta t}$ into Eq. (25), we get the numerical susceptibility as

$$\tilde{\chi}(\omega) = \frac{P(\omega)}{\epsilon_0 E(\omega)} = \frac{e^{i\Delta t\omega}h_0 + h_1 + e^{-i\Delta t\omega}h_2}{e^{i\Delta t\omega}g_0 + g_1 + e^{-i\Delta t\omega}g_2} \quad (26)$$

where "˜" indicates the numerical representation of the quantity.

4.1. Numerical Susceptibility of PLRC Implementation

In the PLRC scheme, the polarization field at a time-step n is expressed as [11]

$$\mathbf{P}^n = \epsilon_0 \sum_{m=0}^{n-1}\left(\mathbf{E}^{n-m}\chi^m + \left(\mathbf{E}^{n-m-1} - \mathbf{E}^{n-m}\right)\xi^m\right). \quad (27)$$

By converting Eq. (27) to the form of Eq. (25) and by comparing the coefficients, we get

$$\begin{aligned}
g_1 &= \frac{\xi^m\chi^{m-2} - \xi^{m-2}\chi^m}{\xi^{m-1}\chi^m - \xi^m\chi^{m-1}}g_0 \\
g_2 &= \frac{\xi^{m-2}\chi^{m-1} - \xi^{m-1}\chi^{m-2}}{\xi^{m-1}\chi^m - \xi^m\chi^{m-1}}g_0 \\
h_0 &= \xi^0 g_1 + \xi^1 g_2 \\
h_1 &= \left(\chi^0 - \xi^0\right)g_1 + \left(\chi^1 + \xi^0 - \xi^1\right)g_2 \\
h_2 &= \left(\chi^0 - \xi^0\right)g_2.
\end{aligned} \quad (28)$$

Using the results of Section 2.1.1, the numerical electric susceptibility of Drude term of the PLRC implementation can be

written as

$$\tilde{\chi}_D^{\mathrm{PLRC}}(\omega) = \chi_D(\omega) - \frac{\omega^2 \chi_D(\omega)}{12}\Delta t^2 + O\left(\Delta t^3\right). \tag{29}$$

Similarly, by using the results of Section 2.1.2, the numerical electric susceptibility of critical term, $\tilde{\chi}_p^{\mathrm{PLRC}}(\omega)$ of the PLRC implementation is given by

$$\tilde{\chi}_p^{\mathrm{PLRC}}(\omega) = \chi_p(\omega) - \frac{\omega^2 \chi_p(\omega)}{12}\Delta t^2 + O\left(\Delta t^3\right). \tag{30}$$

It can be seen that the second order relative errors of the PLRC implementations are independent on the parameters of the DCP model, i.e., material property. Also, Fig. 3 shows that the relative error increases as the frequency increases. This is because for higher frequencies, a higher sampling ratio is required to maintain the same accuracy. In other words, for a fixed time-stepping size, the relative error will increase as the frequency increases.

4.2. Numerical Susceptibility of ADE Implementation

By a direct comparison of Eq. (25) with Eqs. (19) and (21), we can obtain the coefficients of numerical susceptibilities for Drude and critical point poles, respectively. The numerical electric susceptibility for the Drude term of ADE implementation is

$$\tilde{\chi}_D^{\mathrm{ADE}}(\omega) = \chi_D(\omega) - \frac{\omega^2(i\gamma + 2\omega)\chi_D(\omega)}{12(i\gamma + \omega)}\Delta t^2 + O\left(\Delta t^4\right). \tag{31}$$

Also, the numerical electric susceptibility for critical point term of ADE implementation is

$$\begin{aligned}\tilde{\chi}_p^{\mathrm{ADE}}(\omega) \;=\; & \chi_p(\omega) - \frac{\omega^3 \chi_p(\omega)}{12}\left(\frac{1}{\omega + i\Gamma_p - \Omega_p} + \frac{1}{\omega + i\Gamma_p + \Omega_p}\right. \\ & \left. - \frac{1}{\omega + i\Gamma_p - i\Omega_p \cot\phi_p}\right)\Delta t^2 + O\left(\Delta t^4\right). \end{aligned} \tag{32}$$

The relative error of ADE implementation is generally proportional to the square of frequency like the PLRC implementation. However, there is a peak in the magnitude of relative error at Ω_p corresponding to a pole. The existence of this pole degrades the accuracy of ADE implementation compared to the PLRC scheme for noble metals under study, as shown in Fig. 3.

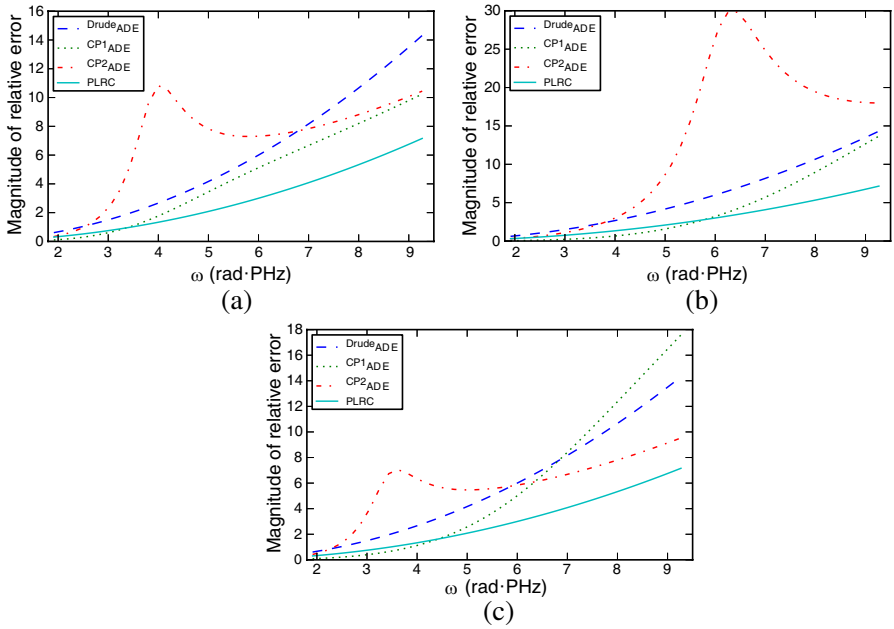

Figure 3. Frequency distribution of relative error of electric susceptibility magnitude from PLRC and ADE implementations of DCP model. CP1 and CP2 indicate the first and second critical points, respectively. For PLRC, the relative error for only one term is displayed since the relative errors of all terms are identical to each other. Δt is set to 1 and the other parameters are listed in Table 1. (a) Gold. (b) Silver. (c) Copper.

5. STABILITY ANALYSIS

Stability is one of the important criteria to be satisfied by the dispersive model when implemented into an FDTD algorithm. A stable system is a system where the errors that occur while solving the finite-difference equations of the FDTD scheme with dispersive models decay as time progresses, thereby not causing the simulation results to diverge.

The combination of the von Neumann method with the Routh-Hurwitz criterion [22] is used to derive the closed-form stability conditions for the FDTD representation of DCP media. As a result, the conditions that make Eq. (25) stable for the Drude pole are

$$\begin{aligned} s_1 &\geq 0 \\ s_2 &\geq 0 \\ s_2 s_3 - s_1 s_4 &\geq 0 \\ s_4 &\geq 0 \end{aligned} \tag{33}$$

and for a critical point are

$$\begin{aligned} s_0 &\geq 0 \\ s_1 &\geq 0 \\ s_1 s_2 - s_0 s_3 &\geq 0 \\ s_1 s_2 s_3 - s_0 s_3^2 - s_1^2 s_4 &\geq 0 \\ s_4 &\geq 0 \end{aligned} \tag{34}$$

where

$$\begin{aligned} s_0 &= \nu^2 \left(g_0 + g_1 + g_2\right) \epsilon_\infty \\ s_1 &= 2\nu^2 \left(-g_0 + g_2\right) \epsilon_\infty \\ s_2 &= h_0 + h_1 + h_2 + \left(g_0 + \left(1 - 2\nu^2\right) g_1 + g_2\right) \epsilon_\infty \\ s_3 &= -2 \left(h_0 - h_2 + \left(1 - \nu^2\right) \left(g_0 - g_2\right) \epsilon_\infty\right) \\ s_4 &= h_0 - h_1 + h_2 + \left(1 - \nu^2\right) \left(g_0 - g_1 + g_2\right) \epsilon_\infty . \end{aligned} \tag{35}$$

The parameter ν is defined as

$$\nu^2 = (c_\infty \Delta t)^2 \left(\frac{\sin^2 \frac{\tilde{k}_x \Delta x}{2}}{\Delta x^2} + \frac{\sin^2 \frac{\tilde{k}_y \Delta y}{2}}{\Delta y^2} + \frac{\sin^2 \frac{\tilde{k}_z \Delta z}{2}}{\Delta z^2} \right) \tag{36}$$

where $c_\infty = (\mu \epsilon_\infty \epsilon_0)^{-1/2}$, $\tilde{k}_{x,y,z}$ are the spatial components of the numerical wavevector, Δx, Δy and Δz are the spatial differences along x, y and z directions, respectively.

The stability condition for the ADE implementation of the Drude pole is

$$0 \leq \nu^2 \leq 1 \tag{37}$$

and is the same as the condition for the non-dispersive FDTD case. However, the PLRC implementation of the Drude pole has stricter condition to be satisfied,

$$0 \leq \nu^2 \leq 1 + \left[\frac{\omega_D^2}{\gamma^3 \Delta t \epsilon_\infty} \left(-\gamma \Delta t + 2 \tanh \frac{\gamma \Delta t}{2} \right) \right]. \tag{38}$$

The terms inside the square brackets will always be negative, and hence the range of ν^2 will be more restricted than Eq. (37).

For the ADE implementation of the critical point, provided that the conditions

$$\sin \phi_p \leq 0 \tag{39}$$

and

$$\left(\Gamma_p^2 - \Omega_p^2\right) \sin \phi_p \leq 2 \Gamma_p \Omega_p \cos \phi_p \tag{40}$$

are satisfied, the stability condition will be the same as that of the non-dispersive FDTD case.

6. FITTING PARAMETERS FOR DCP MODEL OF NOBLE METALS

A fitting procedure was performed to confirm the feasibility of our implementation of the DCP model in correctly representing the dielectric constants of noble metals. The parameters of noble metals

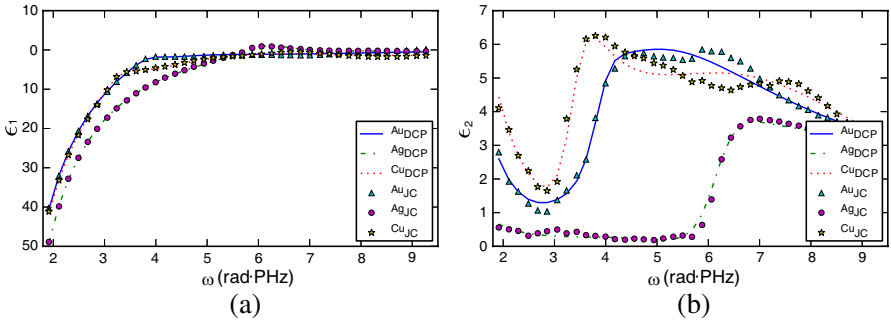

Figure 4. Permittivity of noble metals and its description using DCP model. The label with JC in the subscript means that the data comes from Johnson and Christy [23]. (a) Real part of the relative electric permittivity of noble metals. (b) Imaginary part of the relative electric permittivity of noble metals.

Table 1. Parameters for the DCP model to fit the dielectric functions of noble metals over the $200 < \lambda < 1000\,\text{nm}$ wavelength range (experimental data from Johnson and Christy [23]). Though these parameters do not satisfy Eq. (40), usage of these parameters does not cause the simulations to diverge.

	gold	silver	copper
ϵ_∞	1.11683	0.89583	1.82307
ω_D (rad · PHz)	13.1839	13.8737	13.3846
γ (rad · PHz)	0.109173	0.0207332	0.163439
A_1	3.04155	1.3735	2.57278
ϕ_1 (rad)	−1.09115	−0.504659	-1.56922×10^{-8}
Ω_1 (rad · PHz)	4.20737	7.59914	6.65296
Γ_1 (rad · PHz)	2.35409	4.28431	3.80643
A_2	0.273221	0.304478	0.638294
ϕ_2 (rad)	−1.18299	−1.48944	−1.22019
Ω_2 (rad · PHz)	3.88123	6.15009	3.39199
Γ_2 (rad · PHz)	0.452005	0.659262	0.472389
Φ	3.6308	1.06454	6.07769

were optimized by minimizing a fitness function Φ defined as

$$\Phi = \sum_{\omega} |\epsilon_{\mathrm{T}}(\omega) - \epsilon(\omega)|^2 \tag{41}$$

where ϵ_T is tabulated values in the range from 200 to 1000 nm given in Johnson and Christy [23]. We set all the parameters of the DCP model to have non-negative values except ϕ_p, that was set in the range of $-\pi \leq \phi_p \leq 0$ to satisfy Eq. (39). The optimized parameters of the DCP model for noble metals are shown in Table 1. Note that the parameters shown in Table 1 do not satisfy Eq. (40). We did not choose the optimized parameters that satisfy Eq. (40), because their fitness values are 1.2–4.5 times higher than that of the parameters in Table 1. The real and imaginary values of relative electric permittivity obtained through fitting and experiments are plotted in Fig. 4. A good agreement is observed between the experimental value in Johnson and Christy [23] and the DCP model for various noble metals with our optimized parameters.

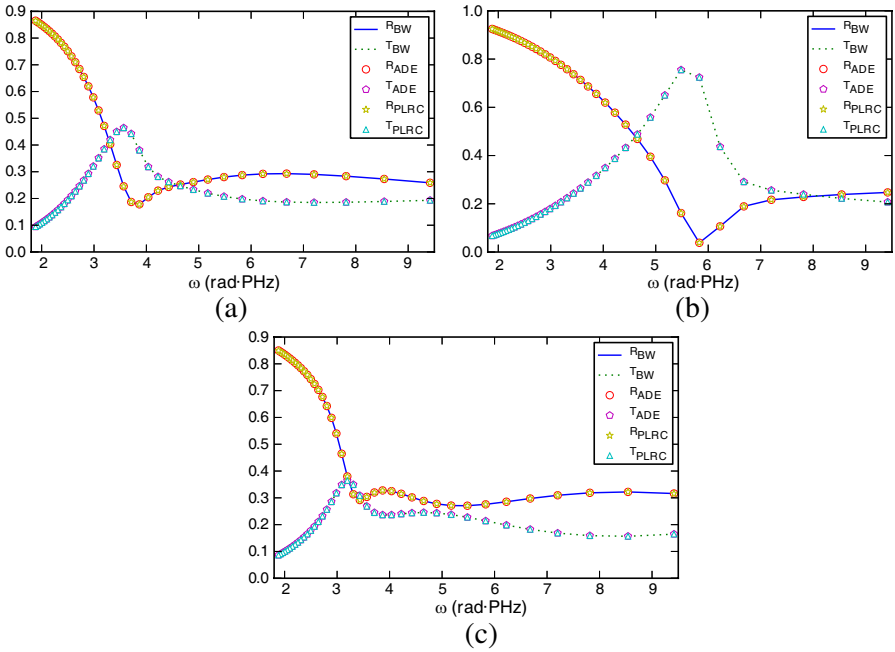

Figure 5. Transmittance and reflectance of the normal incidence of light through a thin metal film made of gold, silver, and copper. BW in the label indicates the analytical results from Born and Wolf [24]. (a) Gold. (b) Silver. (c) Copper.

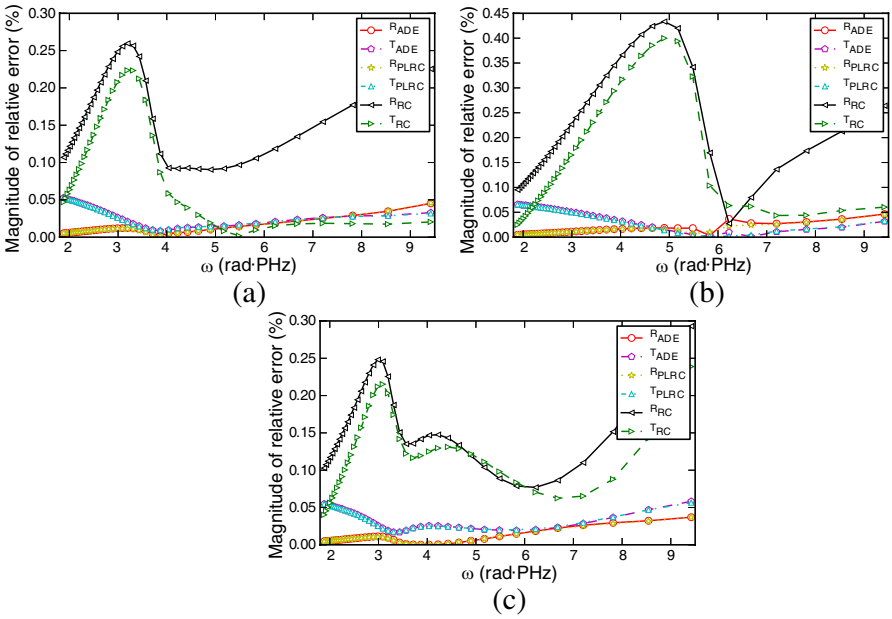

Figure 6. Relative error of transmittance and reflectance through a thin metal film for various metals in ADE, PLRC, and RC schemes. (a) Gold. (b) Silver. (c) Copper.

7. NUMERICAL EXPERIMENTS

The PLRC and ADE schemes for the DCP model have been implemented using an inhouse-developed FDTD package called GMES[†]. The validation of our implementation was done by performing numerical experiments in which the transmission and reflection of light by a thin metal film was studied. Using the parameters given in Table 1, we computed the transmittance and reflectance of light through a thin film made of noble metals surrounded by air as a function of the incident light frequency. A continuous wave source was used as excitation, and the simulations were performed repeatedly with different frequencies to obtain the frequency response over a wide range of frequencies. Since we considered only the normal incidence of light on the metal films, a 1-dimensional space was chosen for the calculation domain. The FDTD parameters are $\Delta x = 1\,\text{nm}$, $\Delta t = \Delta x/(2c)$ where c is the speed of light in vacuum. The numerical results were compared to the results from the analytical method [24]. As shown in Fig. 5, an excellent agreement is observed between the numerical and analytic

[†] http://sourceforge.net/projects/gmes

results for all the metals and implementation schemes considered (ADE and PLRC), which validates our implementation schemes.

In order to further compare the implemented schemes, magnitude of the relative errors for various implementations are plotted in Fig. 6 for the case of gold, silver, and copper. In this case, apart from the ADE and PLRC schemes, the comparison was done for RC scheme by setting the ξ related terms to 0 as discussed in Section 2.1. As seen from Fig. 6, the relative error for reflectance and transmittance of the ADE and PLRC schemes are much lower compared to that of RC scheme for all the metals, except in the case of gold where the RC scheme shows lower errors for transmittance for frequencies above 5 rad·PHz. It is observed that the maximum error of reflectance and transmittance from ADE and PLRC implementations are less than 0.066% which are much lower than that from RC implementation (0.433%).

8. CONCLUSIONS

We have shown the implementations of DCP model for describing dispersive media using the PLRC and ADE schemes into the FDTD algorithm. It was shown that the DCP model can efficiently and accurately describe the experimentally reported permittivity values for various metals. Comparison results of the PLRC and ADE implementations showed that the PLRC scheme requires lesser memory, while the ADE scheme requires relatively fewer arithmetic operations thereby reducing the computational complexity. It was found that the numerical error of the PLRC implementation was less compared to that of the ADE implementation for the metals considered in this paper. Stability analysis of both schemes showed that the ADE scheme can have the same stability condition to that of the non-dispersive FDTD case. Finally, the two implementation schemes were applied in studying the transmittance and reflectance of thin metal films, and excellent agreement was observed between the analytical and numerical results, thus validating our implementations.

ACKNOWLEDGMENT

This work was partially supported by BK-21 Information Technology Project and Basic Science Research Program through the National Research Foundation of Korea (NRF) funded by the Ministry of Education, Science and Technology (NCRC grant No. R15-2008-006-03001-0), Republic of Korea. We also appreciate Sooraj Ravindran of School of Information and Mechatronics for technical discussions and assistance to complete this article.

REFERENCES

1. Ozbay, E., "Plasmonics: Merging photonics and electronics at nanoscale dimensions," *Science*, Vol. 311, No. 5758, 189–193, 2006.
2. Liaw, J.-W., C.-S. Chen, and J.-H. Chen, "Plasmonic effect of gold nanospheroid on spontaneous emission," *Progress In Electromagnetic Research B*, Vol. 31, 283–296, 2011.
3. Smajic, J., C. Hafner, L. Raguin, K. Tavzarashvili, and M. Mishrikey, "Comparison of numerical methods for the analysis of plasmonic structures," *J. Comput. Theor. Nanos.*, Vol. 6, No. 3, 763–774, 2009.
4. Taflove, A. and S. C. Hagness, *Computational Electrodynamics: The Finite-difference Time-domain Method*, 3rd Edition, Artech House Publishers, 685 Canton Street, Norwood, MA 02062, USA, 2005.
5. Lee, K. H., I. Ahmed, R. S. M. Goh, E. H. Khoo, E. P. Li, and T. G. G. Hung, "Implementation of the FDTD method based on lorentz-drude dispersive model on GPU for plasmonics applications," *Progress In Electromagnetic Research*, Vol. 116, 441–456, 2011.
6. Shahmansouri, A. and B. Rashidian, "GPU implementation of split-field finite-difference time-domain method for drude-lorentz dispersive media," *Progress In Electromagnetic Research*, Vol. 125, 55–77, 2012.
7. Etchegoin, P. G., E. C. Le Ru, and M. Meyer, "An analytic model for the optical properties of gold," *J. Chem. Phys.*, Vol. 125, No. 16, 164705-3, 2006.
8. Young, J. L. and R. O. Nelson, "A summary and systematic analysis of FDTD algorithms for linearly dispersive media," *IEEE Antennas Propag. Mag.*, Vol. 43, No. 1, 61–126, 2001.
9. Etchegoin, P. G., E. C. Le Ru, and M. Meyer, "Erratum: 'An analytic model for the optical properties of gold' [*J. Chem. Phys.*, Vol. 125, 164705, 2006]," *J. Chem. Phys.*, Vol. 127, No. 18, 189901-1, 2007.
10. Vial, A. and T. Laroche, "Comparison of gold and silver dispersion laws suitable for FDTD simulations," *Appl. Phys. B*, Vol. 93, No. 1, 139–143, 2008.
11. Kelley, D. F. and R. J. Luebbers, "Piecewise linear recursive convolution for dispersive media using FDTD," *IEEE Trans. on Antennas and Propag.*, Vol. 44, No. 6, 792–797, 1996.
12. Luebbers, R., D. Steich, and K. Kunz, "FDTD calculation of scattering from frequency-dependent materials," *IEEE Trans. on*

Antennas and Propag., Vol. 41, No. 9, 1249–1257, 1993.

13. Vial, A., "Implementation of the critical points model in the recursive convolution method for modelling dispersive media with the finite-difference time domain method," *J. Opt. A: Pure Appl. Opt.*, Vol. 9, No. 7, 745–748, 2007.
14. Sullivan, D. M., *Electromagnetic Simulation Using the FDTD Method*, IEEE Press, 2000.
15. Weedon, W. H. and C. M. Rappaport, "A general method for FDTD modeling of wave propagation in arbitrary frequency-dispersive media," *IEEE Trans. on Antennas and Propag.*, Vol. 45, No. 3, 401–410, 1997.
16. Joseph, R. M., S. C. Hagness, and A. Taflove, "Direct time integration of Maxwell's equations in linear dispersive media with absorption for scattering and propagation of femtosecond electromagnetic pulses," *Opt. Lett.*, Vol. 16, No. 18, 1412–1414, 1991.
17. Okoniewski, M., M. Mrozowski, and M. A. Stuchly, "Simple treatment of multi-term dispersion in FDTD," *IEEE Microw. Guided Wave Lett.*, Vol. 7, No. 5, 121–123, 1997.
18. Vial, A. and T. Laroche, "Description of dispersion properties of metals by means of the critical points model and application to the study of resonant structures using the FDTD method," *J. Phys. D: Appl. Phys.*, Vol. 40, No. 22, 7152–7158, 2007.
19. Okoniewski, M. and E. Okoniewska, "Drude dispersion in ADE FDTD revisited," *Electron. Lett.*, Vol. 42, No. 9, 503–504, 2006.
20. Hulse, C. and A. Knoesen, "Dispersive models for the finite-difference time-domain method: Design, analysis, and implementation," *J. Opt. Soc. Am. A*, Vol. 11, No. 6, 1802–1811, 1994.
21. Lin, Z. and L. Thyln, "On the accuracy and stability of several widely used FDTD approaches for modeling lorentz dielectrics," *IEEE Trans. on Antennas and Propag.*, Vol. 57, No. 10, 3378–3381, 2009.
22. Pereda, A., L. A. Vielva, A. Vegas, and A. Prieto, "Analyzing the stability of the FDTD technique by combining the von Neumann method with the Routh-Hurwitz criterion," *IEEE Trans. on Microw. Theory and Tech.*, Vol. 49, No. 2, 377–381, 2001.
23. Johnson, P. B. and R. W. Christy, "Optical constants of the noble metals," *Phys. Rev. B*, Vol. 6, No. 12, 4370, 1972.
24. Born, M. and E. Wolf, *Principles of Optics: Electromagnetic Theory of Propagation*, 7th Edition, Interference and Diffraction of Light Cambridge University Press, 1999.